(ii) Traveling surface plasmon polariton at metal - dielectric/vacuum interface

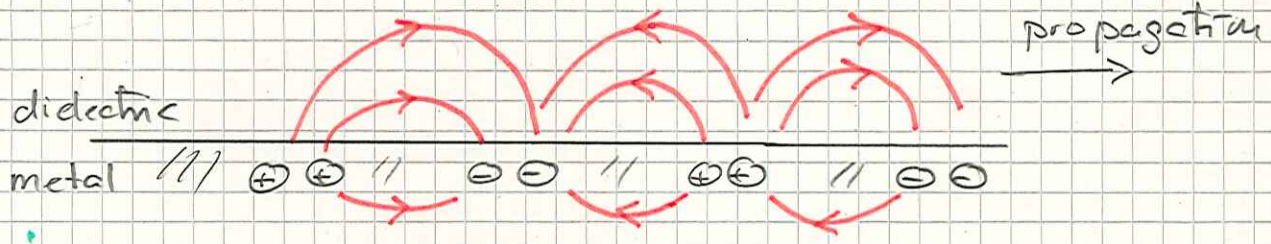

(iii) XUV surface photoemission. Surface & bulk plasmon excitation (surface wake potential)

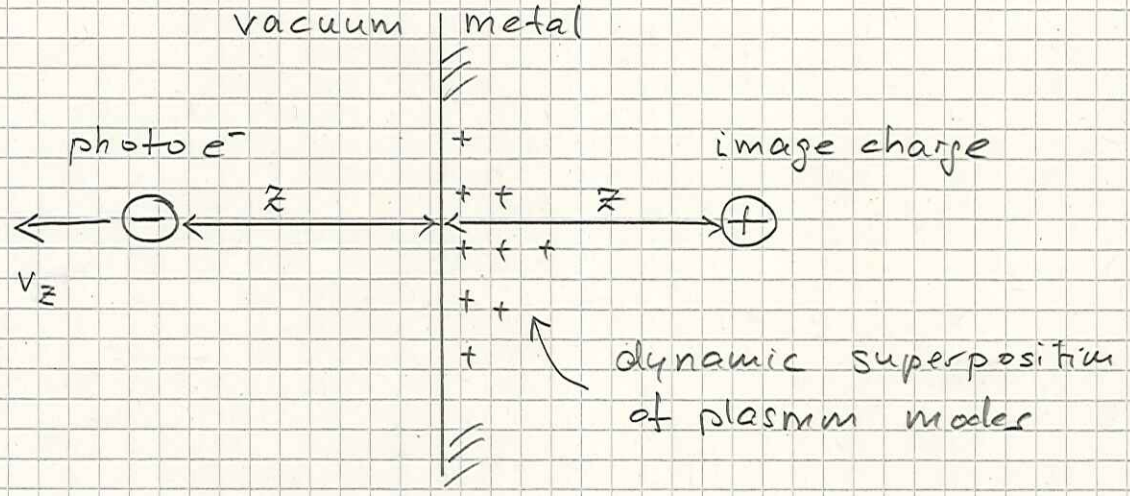

Contribution of dynamical surface charge (image charge) build-up to photo e⁻ streaking delay

Compare

$$V_{im}^{static}(z) = -\frac{1}{4z}$$

static image charge potential ≙ instantaneous electron self-interaction

$$V_{im}^{dyn}(z, v_z) \longrightarrow V_{im}^{static}(z)$$

large z, small v_z

effective potential on PE due to plasmon response

Calculation of plasmon response :

Hamiltonian

creation / annihilation operators

$$H_0 = \underbrace{\sum_{\vec{k},\, k_z \geq 0} \omega_k \, b^+_{\vec{k}} \, b_{\vec{k}}}_{\text{bulk plasmons}} + \underbrace{\sum_{\vec{Q} \in \text{surface plane}} \sigma_Q \, a^+_{\vec{Q}} \, a_{\vec{Q}}}_{\text{surface plasmons}}$$

Dispersion relations (including: plasmon + single-particle excitation)

$$\omega_k = \left(\omega_p^2 + 3 k_F^2 k^2 + k^4/4 \right)^{1/2}$$

decay into e^--hole pairs

$$\sigma_Q = \left(\omega_s^2 + \sqrt{3}\, k_F \omega_s Q/\sqrt{5} + \beta Q^2 + Q^4/4 \right)^{1/2}$$

where

$\omega_p = 4\pi n$ (bulk) plasmon frequency

$\omega_s = \omega_p/\sqrt{2}$ surface —"—

n : bulk e^- density

$k_F = (3\pi^2 n)^{1/3}$ Fermi momentum

β : fit parameter, determined to make surface & bulk dispersion merge e^--hole continuum at same momentum and energy

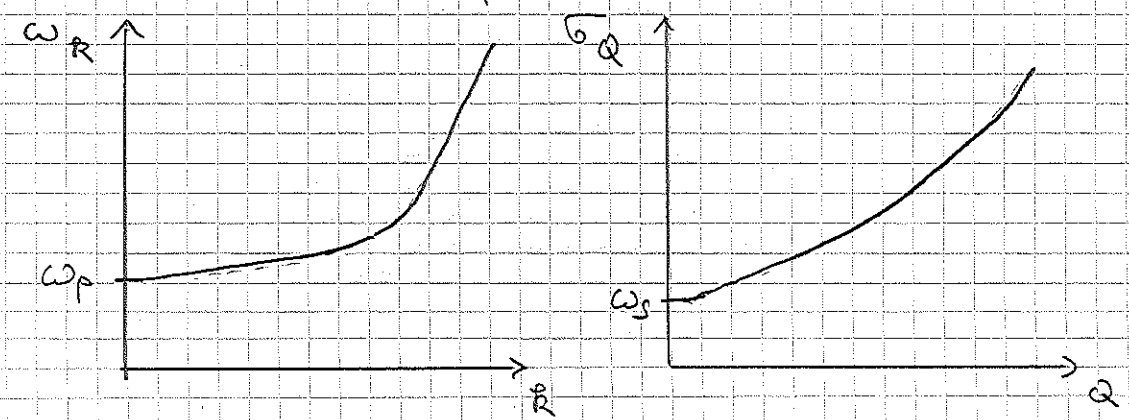

- assume classical photoelectron

$$\rho(\vec{r},t) = -\underbrace{\delta(\vec{r}_\parallel)}_{\text{for emission} \perp \text{ to surface}}\,\delta(z,t) \quad \text{charge density}$$

Interaction by plasmon creation/annihilation

$$H_{int} = \int d\vec{r}\,\rho(\vec{r},t) \times \left[\sum_{\vec{Q}}\left(\frac{\pi\omega_s^2}{AQ\sigma_Q}\right)^{1/2} e^{-Q|z|} e^{i\vec{Q}\cdot\vec{r}_\parallel}\left(a^+_{\vec{Q}} + a_{-\vec{Q}}\right)\right.$$

surface plasmon excitation

$$\left. + \Theta(-z)\sum_{\vec{R},R_z\geq 0}\left(\frac{8\pi\omega_p^2}{VR^2\omega_R}\right)^{1/2}\sin(R_z z)\, e^{i\vec{R}\cdot\vec{r}_\parallel}\left(b^+_{\vec{R}_\parallel,R_z} + b_{-\vec{R}_\parallel,R_z}\right)\right]$$

bulk plasmon excitation

where

A/V = quantization surface / volume

Evolution of initial plasmon field $|\Psi_0\rangle = |\Psi(t=-\infty)\rangle$
(= vacuum state of plasmon field)

$$|\Psi(t)\rangle = \underbrace{T}_{\text{time ordering}} \exp\left[-i\int_{-\infty}^{t} dt'\, \underbrace{e^{iH_0 t} H_{int} e^{-iH_0 t}}_{H_{int}\text{ in interaction picture}}\right] |\Psi_0\rangle$$

this requires some algebra, but can be calculated analytically.

Finally, the dyn. image potential is obtained:

$$V_{im}^{dyn}(z, v_z(t)) = \frac{1}{2}\langle \psi(t)| e^{iH_0 t} H_{int} e^{-iH_0 t} |\psi(t)\rangle$$

$$= \Sigma_r(z, v_z(t)) + i\,\Sigma_i(z, v_z(t))$$

$z \to \infty$, $v_z \to 0$: $\Sigma_r \to -1/(4z)$, $\Sigma_i \to 0$

Handout: Num. example for Al surface, from [1]=Zhang + U.T., Phys. Rev. A 84, 063403 (2011)

(Fig. 1:) - v_z dependent "wake" potential on vacuum side

= wake amplitude ↗ as v_z ↗

- wake amplitude → 0 as $v_z \to 0$.

Compute streaked spectrum for static & dyn. image potentials:

(i) Find eigenfunctions for thick Al slab (typical thickness in num. calc. = 300 a.u.)

$$\left[-\frac{1}{2}\frac{d^2}{dz^2} + U^{static}(z) - \varepsilon_k\right]\psi_k = 0 \quad \text{(short } k \text{ for } k_z\text{)}$$

$$U^{static} = \underbrace{\frac{-11.7\,eV}{1+\exp(z/2.8)}}_{=:U_J(z),\ \text{adjusted to DFT results}} + V_{im}^{static}(z)$$

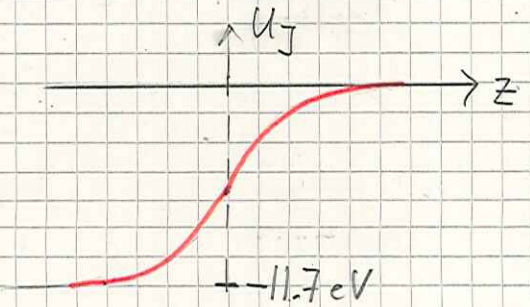

$$\Rightarrow \{\psi_k(z,t) = \psi_k(z)\, e^{-i\varepsilon_k t}\}$$

Towards the time-resolution of collective excitations in solids

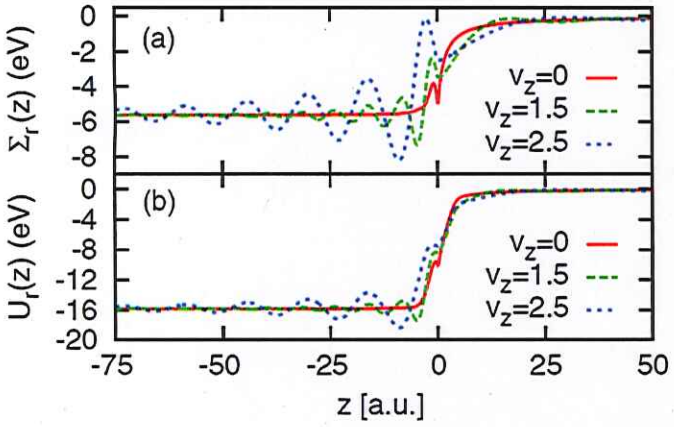

(a) Dynamic wake potential V_{im}^{dyn} for Al for different PE velocities.

(b) Real part of the total surface potential U^{dyn}. The

Streaked XUV photoemission from Al surface

$$\Delta\tau_{dyn} - \Delta\tau_{sta} = 100\ \text{as}$$

Dynamic surface-charge rearrangement $V_{im}(z, v_z)$ → surf.+bulk plasmon excit.

Instant (static) surface charges $V_{im}^{static}(z) = -\frac{1}{4z}$ →

$\hbar\omega_X = 40\ \text{eV}, \hbar\omega_s = 10\ \text{eV}$

$\lambda = 10\ a.u., \delta_L = 0$

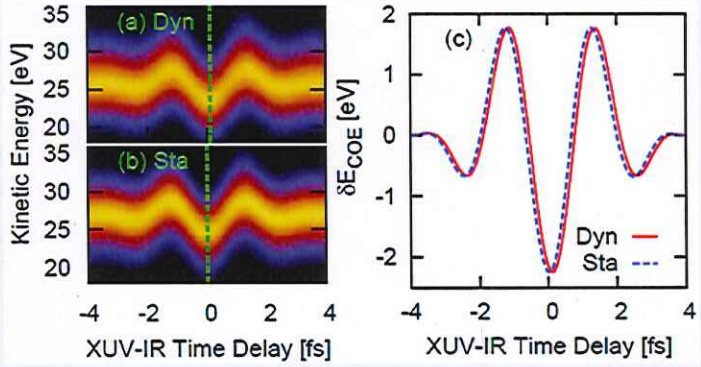

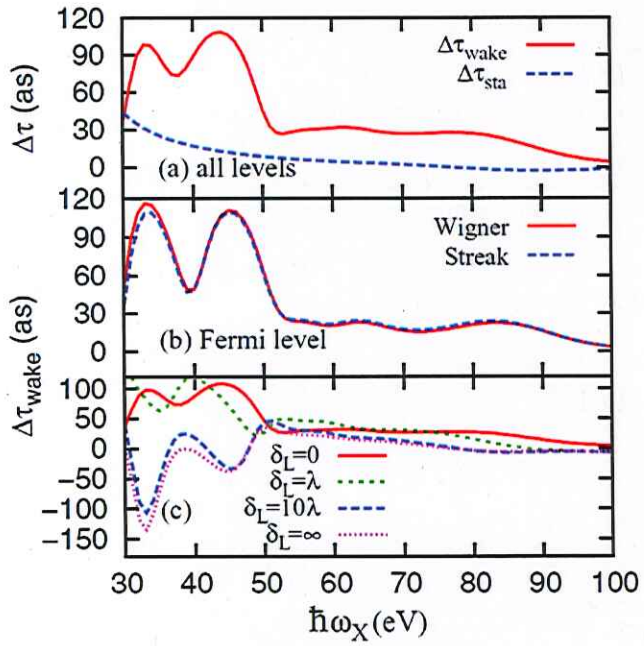

Dependence on the IR skin depth δ_L. "Wigner" refers to the extraction of relative time delays from the PE wave packet center.

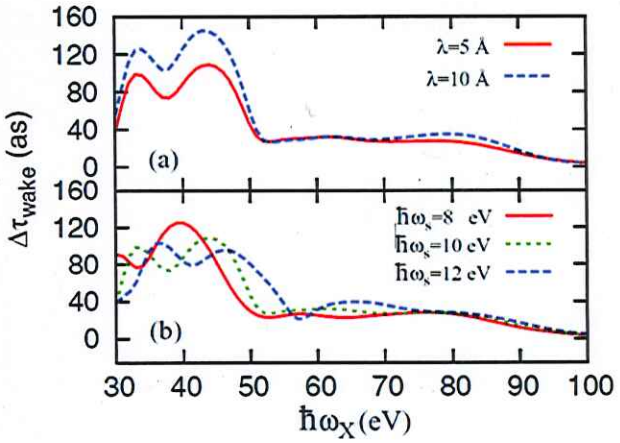

Dependence on (a) the electron mean-free path and (b) surface plasmon energy.

Zhang & U.T., *PRA* **84** (2011)

U.T., Liao, *et al.*, Handbook of Photonics, Vol.**1**, Chap. XIII (Wiley, 2015)

(ii) PE propagation from occupied substrate states $\{\psi_k\}$:

$$i\frac{\partial}{\partial t}\phi_k^{\text{stat/dyn}}(z,t) = \left[\frac{1}{2}\left(-i\frac{\partial}{\partial z} + A_{IR}(z,t)\right)^2 + \begin{Bmatrix} U^{\text{stat}}(z) \\ U^{\text{dyn}}(z, v_z) \end{Bmatrix}\right]\phi_k^{\text{stat/dyn}} + z\,\bar{E}_{XUV}(t+T)\,\psi_k(z,t)$$

surface screened IR streaking field

$k \le k_F$ at 0K

where

$$U^{\text{dyn}} = U_J(z) + V_{im}^{\text{dyn}}(z, v_z)$$

(iii) Photoelectron emission probability ($\hat{=}$ streaked spectrum)

Fourier transform:

$$\tilde{\phi}_k(q,T) = (2\pi)^{-1/2}\int dz \lim_{t\to\infty} \phi_k(z,t)\, e^{-iqz}$$

Incoherently add contributions from occupied states: (here for 0K)

$$P(\varepsilon,T) = \sum_{\varepsilon=\varepsilon(k)<\varepsilon_F} \int dq \left|\tilde{\phi}_k(q,T)\right|^2$$

Time delays

Separately fit centers of energy for calculations with U^{stat} & U^{dyn}:

$$E_{COE}^{\text{stat/dyn}}(T) = a + b\,A_{IR}(t+T)$$

A_{IR}: no z-dependence for $z>0$

$$\Delta T_{\text{wake}} = T^{\text{dyn}} - T^{\text{stat}}$$

Handout: Num. example for Al surface (from [1])

(Fig. 2:) – streaked spectra

– $E_{COE}^{\text{stat/dyn}}(T) \Rightarrow \Delta T_{\text{wake}} \approx 100$ as

C-4 Numerical propagation of photoelectron wave packets

Several of the numerical examples we discussed and will look at rely on wave-function propagation in time and space using a numerical spatial grid. We will therefore outline this powerful numerical method for the simple case of a 1D spatial grid, before studying interferometric photoelectron spectra in section 2D.

- Direct solution of the TDSE on a spatial (position or momentum) grid,

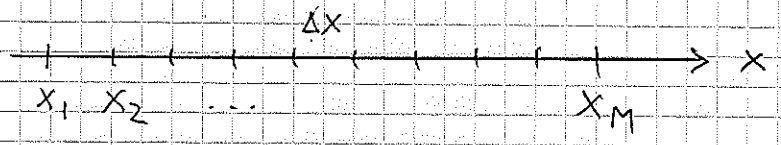

  - assumed equidistant grid spacing Δx
  - method can be extended to $n>1$ dimensions and variable grid spacing
  - wave function and (representations of) operators are mapped on complex numbers associated with grid points $\{x_j\}_{j=1..M}$ at given time steps $\{t_n\}_{n=1..N}$

In general: Integration of the TDSE gives

$$\psi(t) = \hat{T} \exp\left(-i \int_{t_0}^{t} H(t')\, dt'\right) \psi(t_0)$$

$\hat{T}$: time ordering (later to left) — need

exp: expansion leads to products of operators, such as $H(t_1') H(t_2') \cdots H(t_k')$, that don't commute.

Divide $[t_0, t]$ into small time steps τ

$$t_0 < t_1 < \dots < t_N = t$$

$$t_{i+1} - t_i = \tau$$

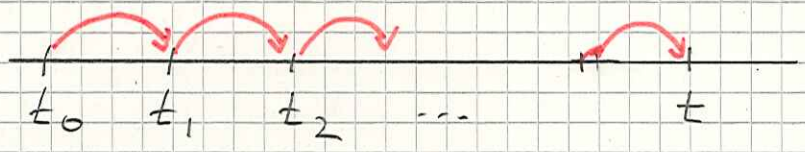

- assume $H(t)$ can be considered time-independent during $[t, t+\tau]$

$$\Rightarrow \quad \psi(t+\tau) = \exp(-i H \tau)\, \psi(t)$$

$$H = -\frac{1}{2}\frac{d^2}{dx^2} + V(x,t)$$

"Finite differencing" puts ψ and H on the spatio-temporal grid:

time $\longrightarrow$ n, space $\longrightarrow$ j

$$\psi_j^n := \psi(x_j, t_n) \; ; \quad V_j^n := V(x_j, t_n)$$

$$i\frac{\partial}{\partial t}\psi(x,t) = H(x,t)\,\psi(x,t)$$

"3 pt formula"

$$i\frac{\psi_j^{n+1} - \psi_j^n}{\tau} = -\frac{1}{2}\frac{\psi_{j+1}^n - 2\psi_j^n - \psi_{j-1}^n}{\Delta x^2} + V_j^n \psi_j^n$$

$$= : \sum_{k=1}^{M} H_{jk}^n \psi_k^n$$

$\hat{H} \hat{=}$ banded (tridiagonal) matrix

$$H_{jk}^n := -\frac{1}{2\Delta x^2}\left(\delta_{k,j+1} - 2\delta_{kj} + \delta_{k,j-1}\right) + V_j^n \delta_{kj}$$

Time propagation (first guess):

$$|\psi^n\rangle := \begin{pmatrix} \psi_1^n \\ \vdots \\ \psi_M^n \end{pmatrix}$$

$M \times M$ banded matrix

$$|\psi^{n+1}\rangle = (\underline{1} - i\tau H^n)\,|\psi^n\rangle + O(\tau^2)$$

Problem: this "explicit" scheme tends to become unstable for "larger" τ

Better: <u>Cayley scheme</u>: num. stable for any τ

- mix of backward & forward propagation

backward prop. ("implicit")

$$\left(\mathbb{1} + i\tau H^n\right)|\psi^{n+1}\rangle = |\psi^n\rangle$$

Cayley:

$$\left(\mathbb{1} + i\frac{\tau}{2}H^n\right)|\psi^{n+1}\rangle = \left(\mathbb{1} - i\frac{\tau}{2}H^n\right)|\psi^n\rangle$$

$$|\psi^{n+1}\rangle = \underbrace{\left(\mathbb{1} + i\frac{\tau}{2}H\right)^{-1}}_{\text{matrix inversion}}\left(\mathbb{1} - i\frac{\tau}{2}H\right)|\psi^n\rangle + O(\tau^3) \quad (*)$$

unitary

Numerics: avoid computing inverse operator.

Instead of

$$2\left(\mathbb{1} + i\frac{\tau}{2}H\right)^{-1}|\chi\rangle = :|\xi\rangle$$

solve linear system of equations for $|\xi\rangle$

$$\frac{1}{2}\left(\mathbb{1} + \frac{\tau}{2}H\right)|\xi\rangle = |\chi\rangle$$

rewrite $(*)$ as

$$|\psi^{n+1}\rangle = \left[2\left(\mathbb{1} + i\frac{\tau}{2}H\right)^{-1} - \mathbb{1}\right]|\psi^n\rangle$$

$$= |\xi\rangle - |\psi^n\rangle$$

<u>Split-operator technique</u>

$$H = T + V(x,t), \quad [T, V] \neq 0$$

$$\psi(t+\tau) = \exp(-i T\tau)\exp(-i V\tau)\psi(\tau) + O(\tau^2)$$

but

$$\psi(t+T) = \exp\left(-i\frac{T}{2}V\right)\exp(-iLT)\exp\left(-i\frac{T}{2}V\right)\psi(t) + O(T^3)$$

← !.

2.D Interferometric photo emission

≙ RABITT spectroscopy

(reconstruction of attosecond beating by interference of two-photon transitions)

↑

or more (→ multiple sidebands)

- Basic idea for single sidebands : two-path interference

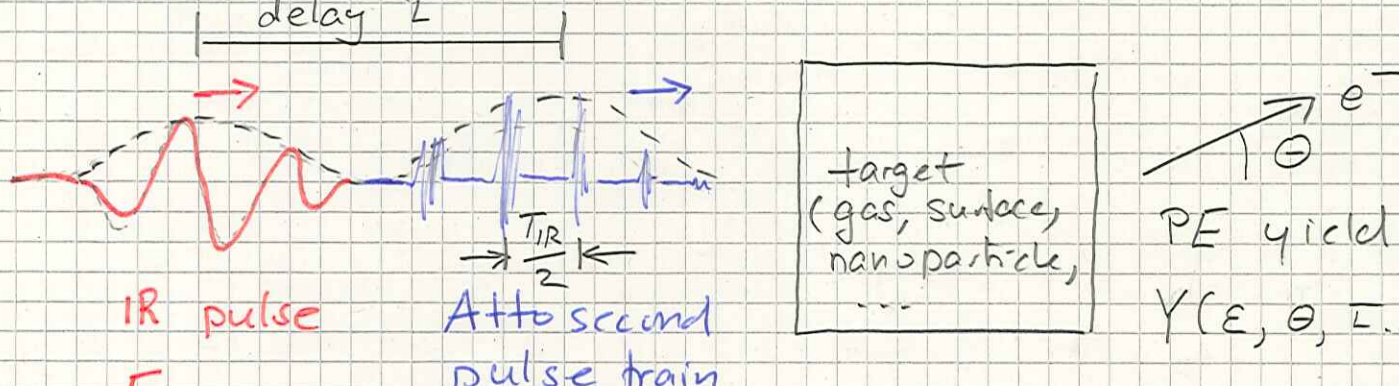

$$E_{XUV} = -\frac{\partial}{\partial t} A_{XUV}(t)$$

$$A_{XUV} = \sum_n A_{XUV}^{2n+1}(t)$$ Superposition of high harmonics

$$A_{XUV}^{2n+1} = a_{XUV}^{2n+1} f_{XUV}^{2n+1}(t)\, e^{i\left(k_{2n+1} r - \omega_{2n+1} t + \phi_{2n+1}^{HH}\right)}$$

$\omega_{2n+1} \rightarrow (2n+1)\,\omega_{IR}$

$a_{xuv}^{2n+1} \in \mathbb{R}$: harmonic amplitude

f_{xuv}^{2n+1} : harmonic envelope, e.g. $\sim e^{-\alpha_{2n+1} t^2}$

ϕ_{2n+1}^{HH} : harmonic phase

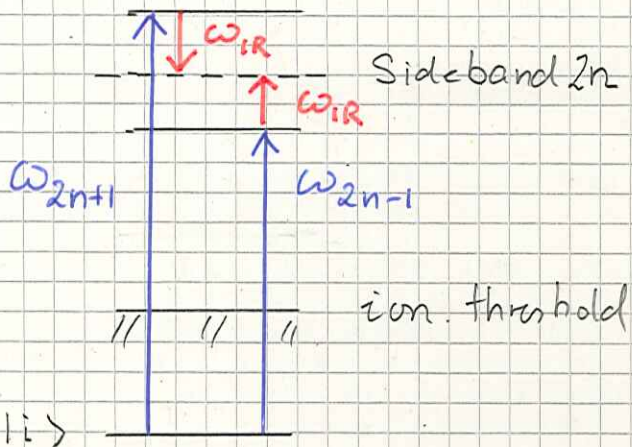

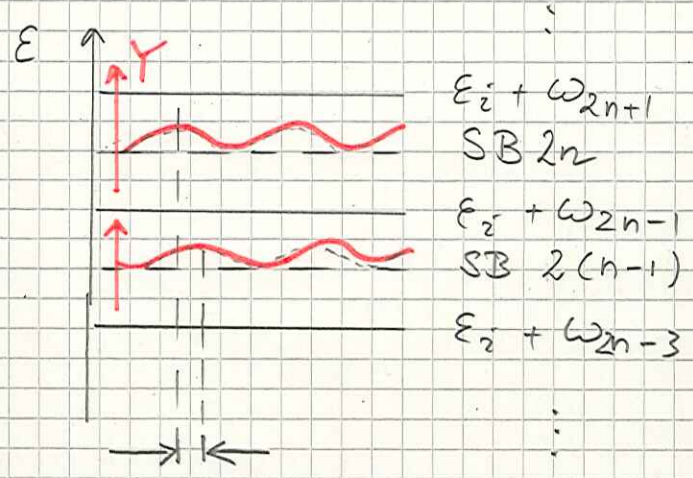

$$\Delta\phi^{RAB} = \phi_{2n}^{RAB} - \phi_{2(n-1)}^{RAB}$$

PE yield near SB 2n

$$Y \sim Y_0 + Y_1 \cos\left(2\omega_{IR} T + \phi_{2n}^{RAB}\right)$$

RABITT phase

$$\phi_{2n}^{RAB} = \phi_{2n-1}^{+} - \phi_{2n+1}^{-} + \underbrace{\phi_{2n+1}^{HH} - \phi_{2n-1}^{HH}}_{\text{usually unknown}}$$

D.1 Gaseous atomic targets

Example: Interferometric photoemission from the 2s & 2p subshells of Ne.

- Isinger et al., Science 358, 893 (2017)

Principle of the interferometric technique. (**A**) Kinetic energy diagram for ionization from the 2s and 2p subshells using XUV (blue arrows) and IR (red arrows) radiation. (**B**) Time-averaged photoelectron spectrum obtained with Al-Zr–filtered harmonics. For both the 2s and 2p subshells, ionization results in three peaks due to absorption of harmonics (H41, H43, and H45) and two sideband peaks (S42 and S44) reachable by two-color two-photon transitions. (**C**) Photoelectron spectrum as a function of delay between the XUV pulse train and the IR field. The sideband amplitudes strongly oscillate as a function of delay.

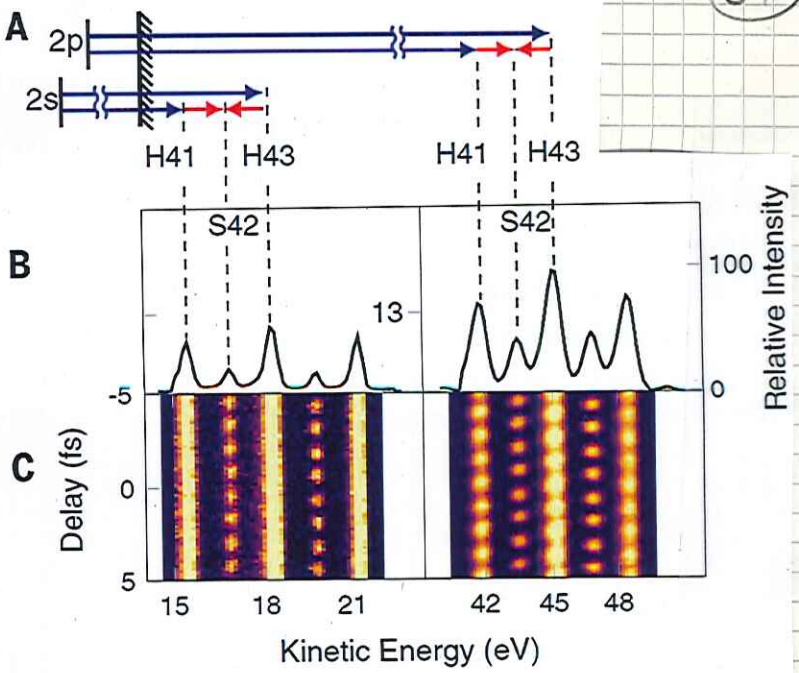

Multi sideband RABITT spectra

Photoionization in the time and frequency domain

Science **358**, 893–896 (2017)

M. Isinger,[1]* R. J. Squibb,[2] D. Busto,[1] S. Zhong,[1] A. Harth,[1] D. Kroon,[1] S. Nandi,[1] C. L. Arnold,[1] M. Miranda,[1] J. M. Dahlström,[1,3] E. Lindroth,[3] R. Feifel,[2] M. Gisselbrecht,[1] A. L'Huillier[1]

We determine photoionization time delays in neon atoms over a 40–electron volt energy range with an interferometric technique combining high temporal and spectral resolution. We spectrally disentangle direct ionization from ionization with shake-up, in which a second electron is left in an excited state, and obtain excellent agreement with theoretical calculations, thereby solving a puzzle raised by 7-year-old measurements.

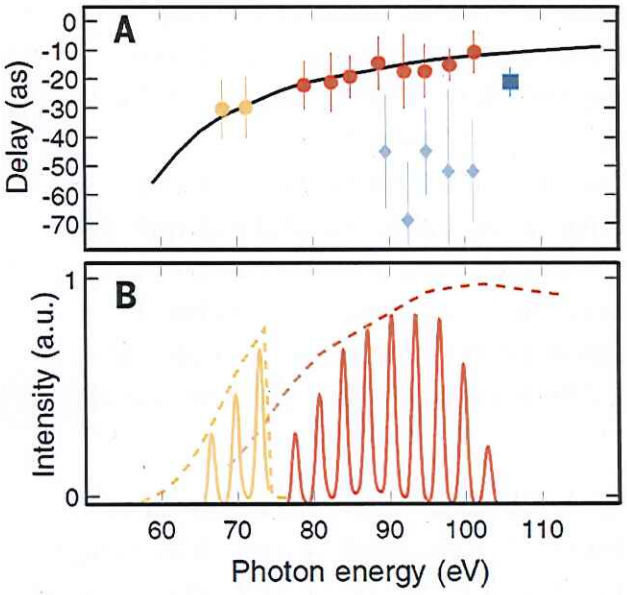

Fig. 1. Photoionization time delays in neon. (**A**) Time delay differences [$\tau_A(2s) - \tau_A(2p)$] in neon as a function of photon energy for the two spectra shown in (B) (yellow and red dots). Theoretical calculations within many-body perturbation theory (black solid line) agree very well with the experimental data. Also shown is the streaking experiment from (*7*) (square), as well as the measured time delay differences [$\tau_A(su) - \tau_A(2p)$] between shake-up and 2p ionization (diamonds). (**B**) Photon spectra used in the measurement. High-order harmonics are generated in neon gas and filtered with a combination of 200-nm-thick Al and Zr filters (yellow spectrum) and with two Zr filters (red spectrum). The dashed lines illustrate the transmission curves of the two combinations of filters (*40*).

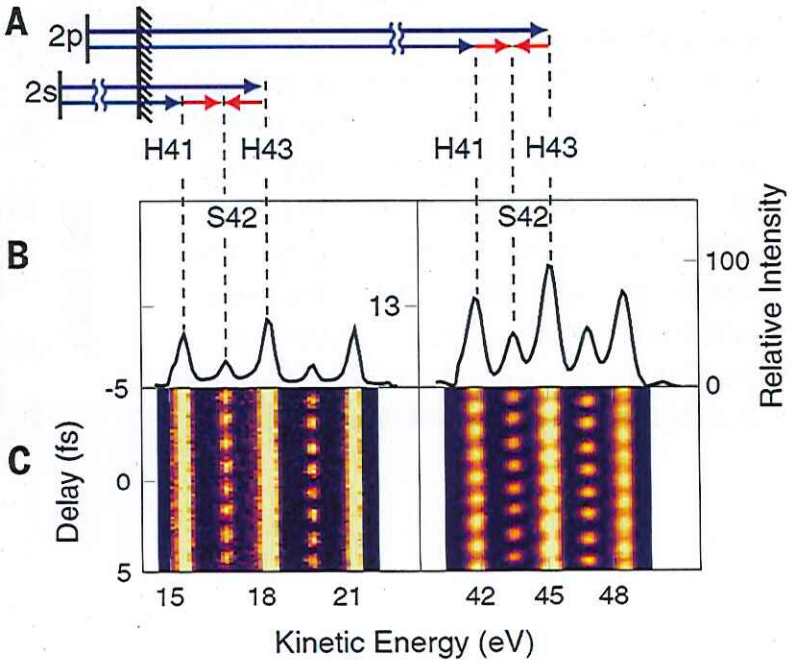

Fig. 2. Principle of the interferometric technique. (**A**) Kinetic energy diagram for ionization from the 2s and 2p subshells using XUV (blue arrows) and IR (red arrows) radiation. (**B**) Time-averaged photoelectron spectrum obtained with Al-Zr–filtered harmonics. For both the 2s and 2p subshells, ionization results in three peaks due to absorption of harmonics (H41, H43, and H45) and two sideband peaks (S42 and S44) reachable by two-color two-photon transitions. (**C**) Photoelectron spectrum as a function of delay between the XUV pulse train and the IR field. The sideband amplitudes strongly oscillate as a function of delay.

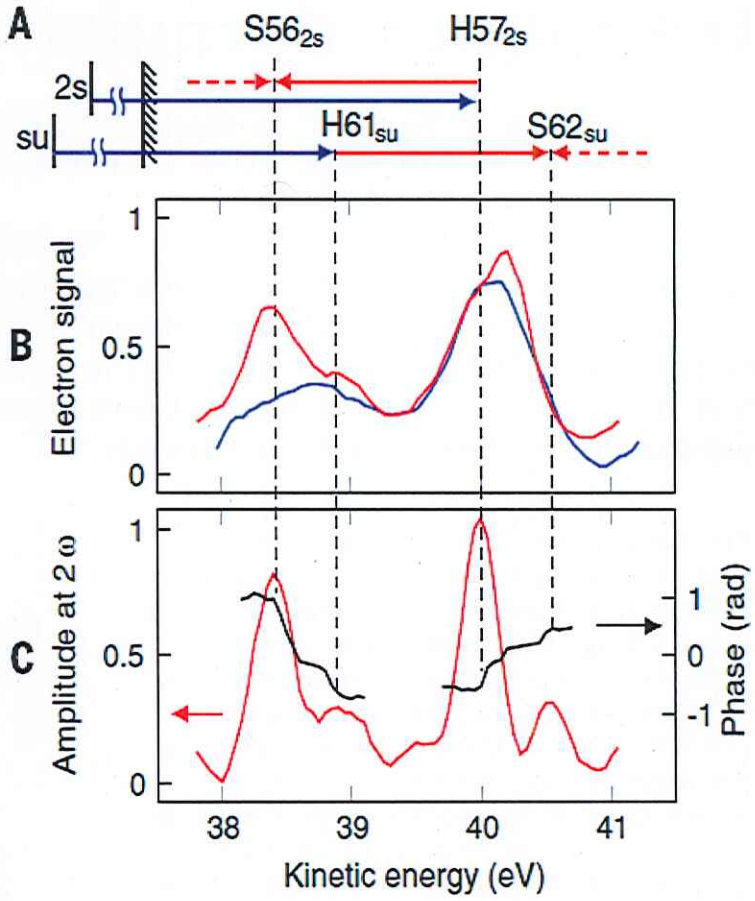

Fig. 3. Energy-resolved interferometric technique and identification of shake-up process. (**A**) Kinetic energy diagram for 2s and 2p ionization accompanied by 2p → 3p excitation (shake-up). The difference in threshold energy for these two processes is approximately 7.4 eV (*11*, *17*). (**B**) Photoelectron spectra obtained with XUV only (blue) and XUV + IR (red). The electron peak due to shake-up induced by absorption of H61 partly overlaps with S56 from 2s ionization. The shoulder on the S56 (red spectrum) can be attributed to one-photon induced shake-up. (**C**) Energy-resolved intensity and phase of the 2ω oscillation, obtained by Fourier transforming the signal. The shake-up harmonic oscillates out of phase with the sideband, causing a sudden drop in the energy-resolved phase. The sideband originating from the shake-up state can be distinguished on the right side, allowing for a separate analysis of its time delay.

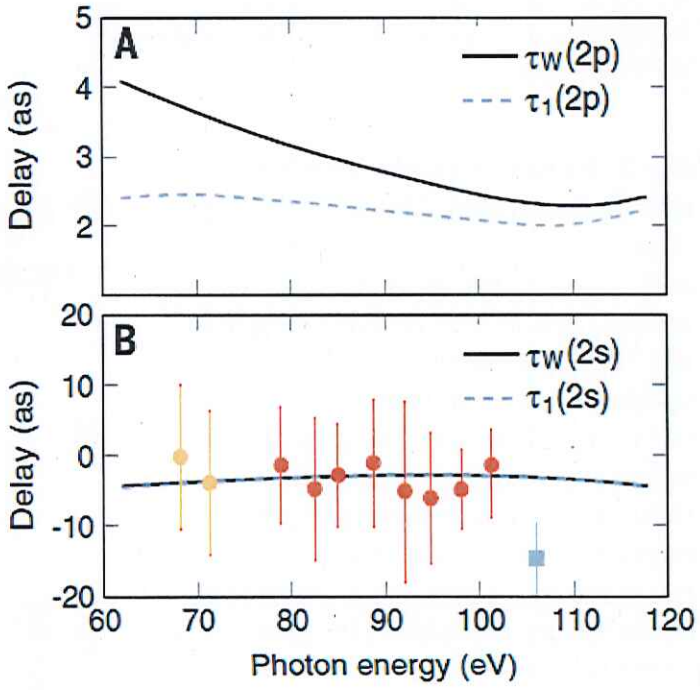

Fig. 4. Absolute photoionization time delays. (**A**) Calculated Wigner delay τ_W(2p) along the direction of the light polarization as a function of the photon energy (black solid line). The dashed line indicates the angle-averaged one-photon ionization time delay accessible in the experiment. The difference between the two quantities is less than two attoseconds over the whole energy range. (**B**) Same as in (A) for 2s ionization. The difference between τ_W(2s) and τ_1(2s) is not visible. The experimental data [this work, yellow and red dots, and (*7*), square] is transformed to τ_1(2s) by subtraction of the analytical τ_{cc}(2s) and simulated τ_1(2p).